International Journal of Computational Methods
Vol. 13, No. 4 (2016) 1641012 (21 pages)
© World Scientific Publishing Company
DOI: 10.1142/S0219876216410127

Int. J. Comput. Methods 2016.13. Downloaded from www.worldscientific.com
by SHANGHAI JIAOTONG UNIVERSITY on 07/27/16. For personal use only.

URANS Studies of Effect of Eccentricity on Ship–Lock Interactions

Qingjie Meng and Decheng Wan*

State Key Laboratory of Ocean Engineering
School of Naval Architecture
Ocean and Civil Engineering, Shanghai Jiao Tong University
Collaborative Innovation Center for Advanced Ship
and Deep-Sea Exploration, Shanghai 200240, P. R. China
dcwan@sjtu.edu.cn

Received 29 September 2015
Accepted 24 December 2015
Published 29 February 2016

The unsteady viscous flow around a 12000TEU ship model entering the Third Set of Panama Locks with different eccentricity is simulated by solving the unsteady Reynolds averaged Navier–Stokes (RANS) equations in combination with the $k-\omega SST$ turbulence model. Overset grid technology is utilized to maintain grid orthogonality and the effects of the free surface are taken into account. The hydrodynamic forces, vertical displacement as well as surface pressure distribution are predicted and analyzed. First, a benchmark test case is designed to validate the capability of the present methods in the prediction of the viscous flow around the ship when maneuvering into the lock. The accumulation of water in front of the ship during entry into a lock is noticed. A set of systematic computations with different eccentricity are then carried out to examine the effect of eccentricity on the ship–lock hydrodynamic interaction.

Keywords: Lock; 12000TEU, overset grid; ship–lock hydrodynamic interaction; eccentricity.

1. Introduction

Scale enlargement in the shipping industry appears to be an ever-lasting trend. Particularly in container transport, the limit is not yet in sight. Nowadays, the 21000 TEU giants are building in China. These evolutions are scrupulously watched by harbor and waterways authorities, who experience the continuous need to evaluate whether new and larger types of ships will still be able to make use of their infrastructure in the future.

The lock approach will always be accompanied with high blockage, since ships can have very small side margins in the lock as well as a very small under keel

*Corresponding author.

clearance. The high blockage influences the flow along the ship hull, increasing the relative speed between the ship and inverse flow. Furthermore, the high blockage also causes a so called piston effect, which provokes an accumulation of water during ship's entry into the lock. The frictional resistance increases and water piles up inside the lock resulting in higher resistance. What is more, it is very difficult to keep the ship maneuvering along the lock's centerline. This obviously produces a worse situation for a ship approaching a lock. Overall, a ship will experience a particular hydrodynamic force caused by the hydrodynamic interaction with the lock, during the entering maneuver into a lock. This hydrodynamic interaction has a significant influence on the ship navigation safety. The investigation on the effects of eccentricity is of crucial importance for safe operation and effective control of ships passing through a lock.

Several methods have been used to examine the feasibility to use locks for large vessels. Although real scale and model scale tests can be carried out, such as Vantorre *et al.* [2012], which is used to validate the present computations, reliable simulations are necessary to examine infrastructure in an affordable and efficient manner. Vrijburcht [1988] used six-waves-model to calculate the translation waves generated by the lock entry. Vergote [2012] improved the six-waves-model. Chen [2010] developed a viscous frictional model to calculate dynamical ship–lock interaction problem. Delefortrie *et al.* [2008, 2009] analyzed the navigation behavior of different ship models in the Third Set of Panama Locks and the influences of approach wall configurations, eccentricities, propeller rates, approaching scenarios and under keel clearances were also discussed. Verwilligen and Richter [2012] investigated the entering maneuver of full form ships into the Terneuzen West Lock by means of model testing, full scale trials and real-time simulations. Very few URANS studies included ship–lock interactions, such as Wang *et al.* [2014], who studied the viscous flow around a ship when entering the Pierre Vandamme Lock based on CFD package Fluent. However, the free-surface simulation was not presented. Meng *et al.* [2015] investigated the effects of the ship speed on the ship–lock interaction by URANS.

The main objective of this study is to examine the effects of eccentricity on a 12000TEU ship model when entering the Third Set of Panama Locks by predicting and analyzing the viscous flow and hydrodynamic forces of the ship model maneuvering into the lock with different lateral position. First, the capability of the present method for the prediction of the viscous flow around the ship model is validated by the good agreement of the predicted results with the corresponding experimental data. Then a series of systematic computations with different lateral position are carried out and the predicted forces and moments, vertical displacement as well as surface pressure distribution are analyzed to investigate the viscous flow around the ship and the influence of the eccentricity on the ship–lock hydrodynamic interaction during its entry into a lock. This study challenges CFD because of low Fr, very restricted water and ship–lock interaction.

The computation is carried out by an in-house CFD code based on the finite difference method (FDM). The code was proved to be competent in simulating the

Int. J. Comput. Methods 2016.13. Downloaded from www.worldscientific.com
by SHANGHAI JIAOTONG UNIVERSITY on 07/27/16. For personal use only.

unsteady viscous flow around a ship in confined water [Meng *et al.* (2014, 2015)]. Finite difference method (FDM) can be used even when high cell aspect ratio is present and thus is very suitable to solve low speed problems. Refinement grids are used only in the vertical direction to ensure the grid number within an acceptable range as well as the accuracy of the capture of the free surface. When a ship moves into a lock, a mass of water will be pushed into the lock. It might cause the accumulation of water in front of the ship, the initial bow up and a significantly increased hydrodynamic forces and moment. So, to make our prediction more reasonable, the effects of the free surface are taken into account. Besides, the overset grid technique is introduced to avoid the deterioration of the computational accuracy caused by the mesh distortion near the boundary layer region when the ship moves with large amplitude.

Int. J. Comput. Methods 2016.13. Downloaded from www.worldscientific.com
by SHANGHAI JIAOTONG UNIVERSITY on 07/27/16. For personal use only.

2. Mathematical Method

2.1. *Governing equations*

The viscous flow around the ship is assumed incompressible and the numerical problem is described by RANS equations coupled with the time-averaged continuity equation in nondimensional tensor form

$$\frac{\partial U_i}{\partial t} + U_j \frac{\partial U_i}{\partial x_j} = -\frac{\partial \hat{p}}{\partial x_i} + \frac{\partial}{\partial x_j}\left[\mathrm{Re}_{\mathrm{eff}}^{-1}\left(\frac{\partial u_i}{\partial x_j} + \frac{\partial u_j}{\partial x_i}\right)\right] + S_i, \tag{1}$$

$$\frac{\partial U_i}{\partial x_i} = 0, \tag{2}$$

where $U_i = (u, v, w)$ denotes the Reynolds-average velocity components; $x_i = (x, y, z)$ represents the independent coordinate directions; S_i stands for a body force due, for instance, to a propeller model, respectively; the piezometric pressure $\hat{p}$ and the effective Reynolds number $\mathrm{Re}_{\mathrm{eff}}$ are:

$$\hat{p} = p_{\mathrm{abs}}/\rho U_0^2 + z/Fr^2 + 2k/3, \tag{3}$$

$$\mathrm{Re}_{\mathrm{eff}}^{-1} = 1/\mathrm{Re} + \gamma_{\mathrm{t}}, \tag{4}$$

where k is the turbulence kinetic energy, p_{abs} is the absolute pressure, z is the local vertical elevation and γ_t is the nondimensional turbulent viscosity obtained from a turbulence model. All the variables and properties are nondimensionalized by the reference velocity U, ship length L_{pp} and the mass density of the water ρ.

2.2. *Turbulence model*

The $k - \omega$ *SST* turbulence model was chosen to close the RANS equations. As the $k - \omega$ *SST* turbulence model employs the $k - \omega$ model near walls and the $k - \varepsilon$ model away from walls, it gives highly accurate predictions of the onset and the amount of flow separation under adverse pressure gradients.

Int. J. Comput. Methods 2016.13. Downloaded from www.worldscientific.com
by SHANGHAI JIAOTONG UNIVERSITY on 07/27/16. For personal use only.

The turbulence kinetic energy k is computed using a blended $k-\varepsilon/k-\omega$ model [Menter (1994)]. In this model, the eddy viscosity ν_t, turbulence kinetic energy k and the turbulence specific dissipation rate ω can be computed from:

$$\nu_t = \frac{k}{\omega}, \tag{5}$$

$$\frac{\partial k}{\partial t} + \left(U_j - \sigma_k \frac{\partial \nu_t}{\partial x_j}\right)\frac{\partial k}{\partial x_j} - \frac{1}{R_k}\nabla^2 k + s_k = 0, \tag{6}$$

$$\frac{\partial \omega}{\partial t} + \left(U_j - \sigma_\omega \frac{\partial \nu_t}{\partial x_j}\right)\frac{\partial \omega}{\partial x_j} - \frac{1}{R_w}\nabla^2 \omega + s_\omega = 0, \tag{7}$$

where the source terms, effective Reynolds numbers, and turbulence production can be described as

$$S_k = R_k(-G + \beta^* \omega k), \tag{8}$$

$$S_\omega = R_\omega\left(-\gamma\frac{\omega}{k}G + \beta\omega^2 + 2(1-F_1)\sigma_{\omega 2}\frac{1}{\omega}\frac{\partial k}{\partial x_j}\frac{\partial \omega}{\partial x_j}\right), \tag{9}$$

$$R_{k/\omega} = \frac{1}{1/\mathrm{Re} + \sigma_{k/\omega}\nu_t}, \tag{10}$$

$$G = \tau_{ij}\frac{\partial u_i}{\partial u_j} = \nu_t[(u_y+v_x)^2 + (u_z+w_x)^2 + (v_z+w_y)^2 + 2u_x^2 + 2v_y^2 + 2w_z^2], \tag{11}$$

with $\beta, \beta^*, \sigma_k, \sigma_\omega$ constants and F_1 the blending function, which is designed to be one in the sub-layer and logarithmic regions of boundary layers and gradually switches to zero in the wake region to take advantage of the strengths of the $k-\omega$ and $k-\varepsilon$ models in different position. The model constants are calculated locally as a weighted average, i.e., $\phi = F_1\phi_1 + (1-F_1)\phi_2$ where ϕ_1 denote the standard $k-\omega$ and ϕ_2 represent $k-\varepsilon$ values.

2.3. *Free surface*

We capture the location of the transient free surface using level set function ϕ [Osher and Sethian (1988); Sussman *et al.* (1994); Sethian and Smereka (2003)], whose value is related to the distance to the interface. And the value of ϕ is arbitrarily set to positive in water and negative in air and the iso-surface $\phi = 0$ represents the free surface. Since the free surface is considered a material interface, then it should satisfy the kinematic free surface boundary condition and can be described as

$$\frac{\partial \phi}{\partial t} + \boldsymbol{\nu}\cdot\nabla\phi = 0. \tag{12}$$

The following conditions for the velocity and pressure should be satisfied

$$\nabla \boldsymbol{v}\cdot\boldsymbol{n} = 0, \tag{13}$$

$$\hat{p} = \frac{z}{Fr^2}, \tag{14}$$

where $\boldsymbol{n} = -\frac{\nabla\phi}{|\nabla\phi|}$ is the unit normal vector to the free surface, pointing from water to air.

To make sure that the level set function is kept a distance function after the transport step, a reinitialization procedure is used in which the points close to the free surface are reinitialized geometrically, while a transport equation is solved for all other points.

3. Simulation Design

The problem under study is a 12000TEU container carrier moving into the Third Set of Panama Lock with different eccentricity. The ship is a 1/80 scale model of 12000TEU. The geometry of the ship model is shown in Fig. 1. A 1/80 scale model of a lock and approach channel is designed according to the preliminary design of the Panama Canal Third Set of Locks. The geometry and the principal dimensions of the lock model is shown in Fig. 2. The geometry is a benchmark on the ship behavior in locks, tested in Flanders Hydraulics Research in 2007–2008. Numerical results are compared with the experimental data by Vantorre *et al.* [2012].

3.1. *Case conditions*

The ship model is $Lpp = 4.35\,\mathrm{m}$ long with $0.19\,\mathrm{m}$ draft. Table 1 gives the principal dimensions of the ship model. Three cases are studied numerically. Case A, with lateral position $\Delta y = 0.0\,\mathrm{mm}$, is designed according to the benchmark test and selected for validation. Numerical tests cases A1 and A2 are also carried out to

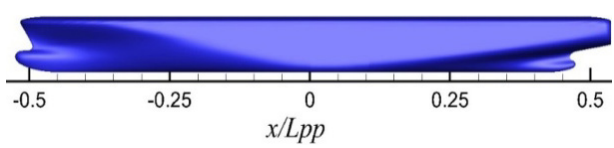

Fig. 1. Geometry of the 12000TEU hull.

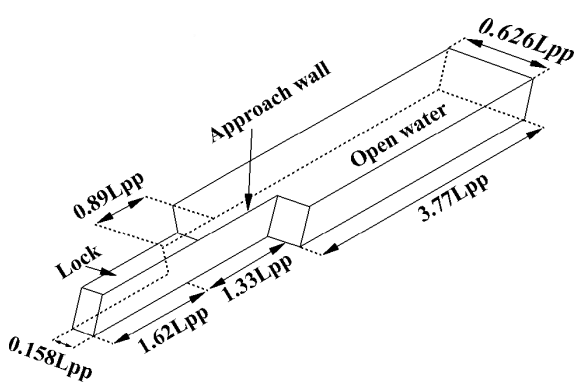

Fig. 2. Geometry of the lock.

Int. J. Comput. Methods 2016.13. Downloaded from www.worldscientific.com
by SHANGHAI JIAOTONG UNIVERSITY on 07/27/16. For personal use only.

Table 1. Principal dimensions of the 12000TEU model.

Item	Symbol	Unit	Value
Length between perpendiculars	L_{pp}	m	4.350
Breadth (molded)	B	m	0.613
Draft (molded)	D	m	0.190
Blockage coefficient	C_B	—	0.65

Table 2. Details of the case conditions.

Conditions			Test No.		
			A	A1	A2
Water depth	h	m	0.228	0.228	0.228
Froude number	Fr	—	0.0176	0.0176	0.0176
Reynolds number	Re	$\times 10^5$	4.392	4.392	4.392
Depth/draft ratio	h/D	—	1.2	1.2	1.2
lateral position	Δy	mm	0.0	7.5	19

Int. J. Comput. Methods 2016.13. Downloaded from www.worldscientific.com
by SHANGHAI JIAOTONG UNIVERSITY on 07/27/16. For personal use only.

study the effects of eccentricity on the hydrodynamic forces acting on the ship, with lateral positions: $\Delta y = 7.5\,\text{mm}$ and $\Delta y = 19\,\text{mm}$ model scale, respectively. Details of the case conditions are shown in Table 2. Free surface is considered for all cases.

3.2. *Computational domain, coordinate system and boundary conditions*

The computational domain, which extends within $-1.62 \leq x \leq 5.10, -0.0524 \leq z \leq 0.17, -0.079 \leq y \leq 0.079$ for the lock and $-0.313 \leq y \leq 0.313$ for the approach channel, covers the whole ship considering the asymmetry of the flow field. A right-handed Cartesian coordinate system is located at the door of the lock. The longitudinal Ox-axis points to the approach channel, the Oz-axis is vertical and points upward, and the undisturbed free surface is taken as the plane $z = 0$. The origin of the coordinates is located at the intersection of the waterline, the center plane of the lock and the plane of the lock door. A schematic diagram indicating the coordinate system and the computational domain is given in Fig. 3. The boundary conditions mimic the conditions in the Flanders hydraulics research (FHR) towing tank for later comparison of the numerical results with the experimental data. The computational domain is made up of three kinds of boundaries: no-slip wall (hull surface), far-field ($z = z_{\max}$) and slip wall (all other boundaries).

3.3. *Grid design*

For all cases, structured grids are used and overset gird technique is utilized to keep the orthogonality of the grid under the consideration of keeping a good computational accuracy.

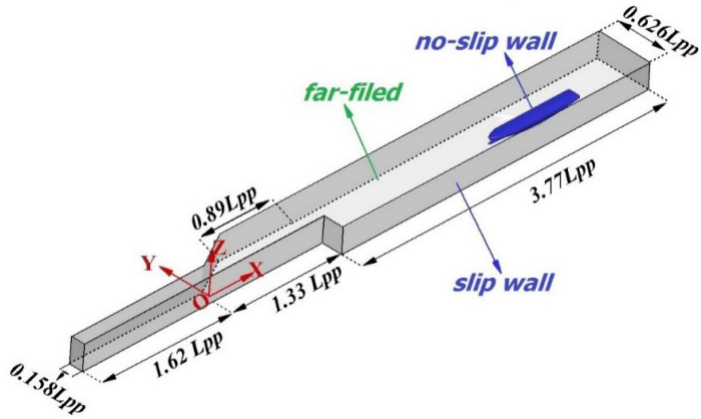

Fig. 3. Computational domain, coordinate system and boundary conditions.

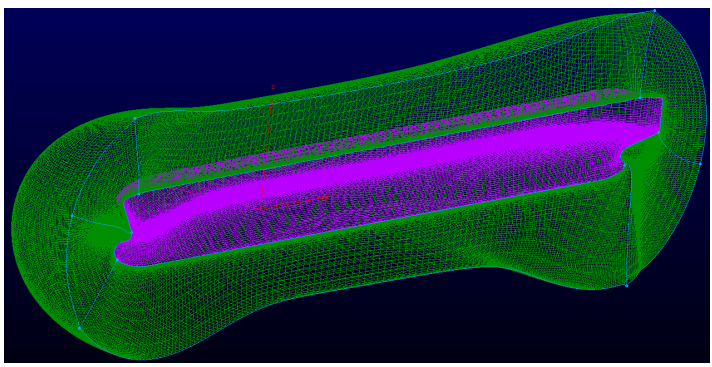

Fig. 4. Boundary layer curvilinear grid of the ship model.

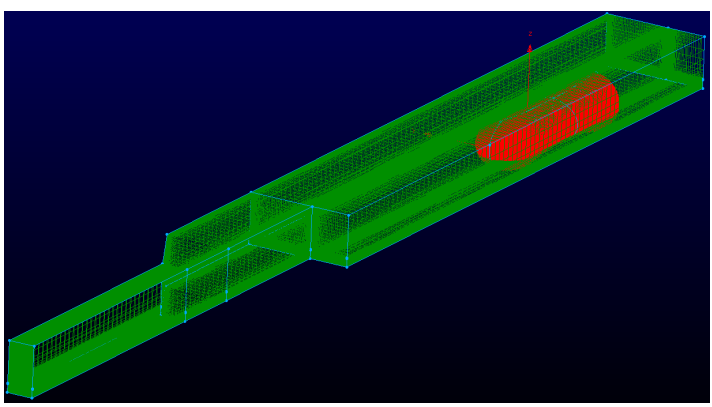

Fig. 5. A sketch of the grid distribution.

Int. J. Comput. Methods 2016.13. Downloaded from www.worldscientific.com
by SHANGHAI JIAOTONG UNIVERSITY on 07/27/16. For personal use only.

Table 3. Summary of the grids used in this study.

Block name (location)	No.	Topology	$i$max × $j$max × $k$max	Grid points
Boundary layer (hull)	2	Double O-grid	159 × 47 × 91	680,043
Background	1	H–H grid	145 × 211 × 101	3,090,095
Total grid points				4,450,181

A sketch of the grid distribution is shown in Figs. 4 and 5, where the grids are coarsened for clarity. The grid consists of a background orthogonal grid, which mimics the towing tank, and a boundary layer curvilinear grid which conforms to the ship geometry where two clusters of grid points are concentrated around the bow and stern regions. The boundary layer grid is generated with a grid spacing at the hull satisfying the condition $y+ < 1$ for all case. All the grids are refined in the vertical direction in $-0.003 \leq z \leq 0.003$, where the free surface is expected. The grids are summarized in Table 3.

4. Results of Benchmark Test Case

Test case A, designed according to the experiment, is used to confirm the capability of present method in the prediction of the viscous flow around the ship model while maneuvering into the lock.

Comparisons between computed and experimental data is presented for the x-direction hydrodynamic force X, y-direction hydrodynamic force Y, the moment around the z-axis N and the vertical displacement of the fore and aft perpendiculars zFP and zAP.

For a clear insight of the viscous flow around the ship during the maneuvering into the lock, three special instants, shown in Fig. 6, are defined. At instant T1, the ship is still moving in the approach channel, while forebody of the ship has entered the lock at instant T2. At instant T3, the ship has entered the lock.

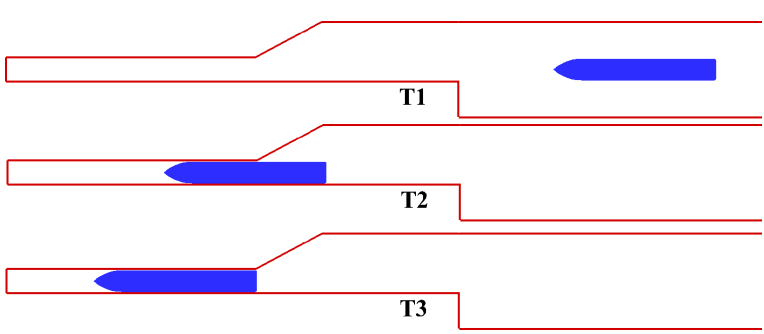

Fig. 6. Definition of three certain times.

Int. J. Comput. Methods 2016.13. Downloaded from www.worldscientific.com
by SHANGHAI JIAOTONG UNIVERSITY on 07/27/16. For personal use only.

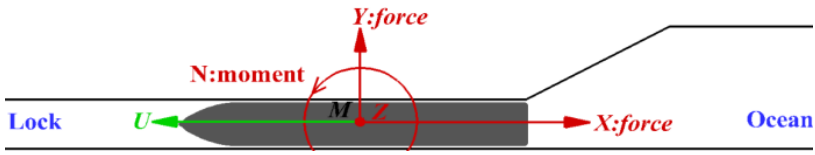

Fig. 7. Coordinate systems for hydrodynamic forces and moment.

4.1. *Hydrodynamic forces*

Coordinate systems for hydrodynamic forces and moment are shown in Fig. 7. Figure 8 presents the comparison of the computed results and experimental data for the time history of hydrodynamic forces and moment, where the x-axis represents the position of the bow. Note that the x coordinate values change from 2.5 to -1 when the ship maneuvering from the approach channel into the lock, as shown by the coordinate system in Fig. 3. The predicted results show good agreement with measured data and exhibits consistent oscillation compared with the experimental data.

Taking longitudinal force X as an example, during maneuverer the ship into the lock, it goes through three stages. In the first stage, the hydrodynamic force X is

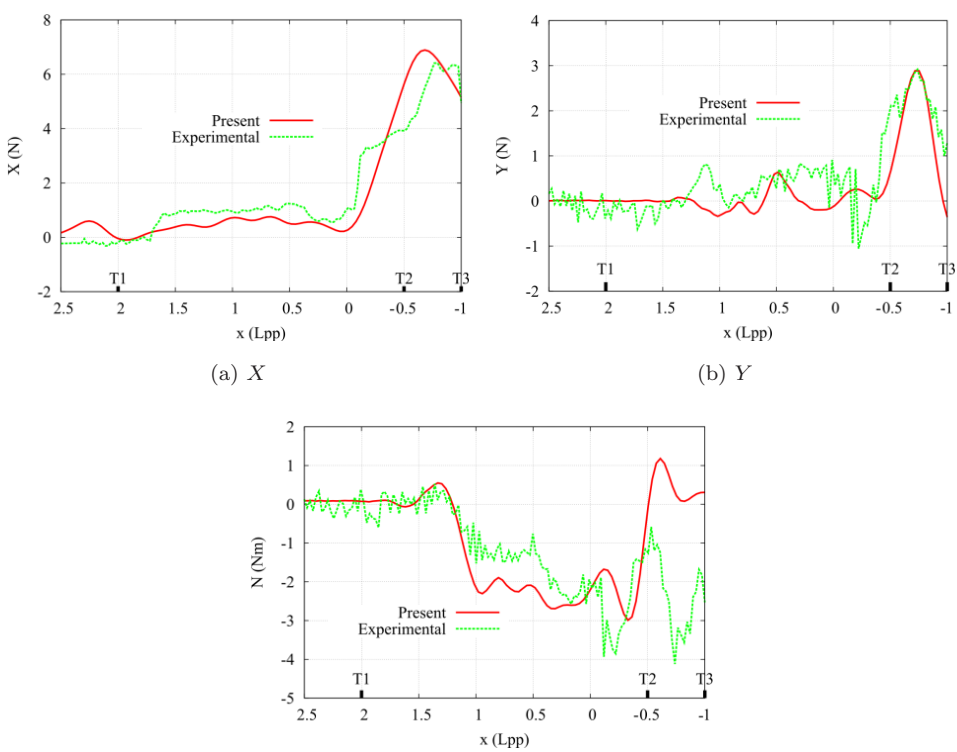

(a) X (b) Y

(c) N

Fig. 8. Time history of the hydrodynamic forces and moment.

Int. J. Comput. Methods 2016.13. Downloaded from www.worldscientific.com
by SHANGHAI JIAOTONG UNIVERSITY on 07/27/16. For personal use only.

very small with insignificant oscillation when the ship maneuvers in the approach channel. This is caused by the extremely low ship speed. Then, a soaring increase of the hydrodynamic force X is noticed during the ship maneuvering into the lock. During the entry into the lock, an accumulation of water is provoked in front of the ship because of the piston effect. This induces the increase of the bow pressure and the decrease of the stern pressure, which causes a dramatically increase of the viscous pressure resistance. Also, an increased friction resistance will occur because of the higher velocities of the return flow. Accordingly, the longitudinal force X increases. At the least stage, once the ship has entered the lock, a significant decrease of the resistance force can be noticed. When the ship has entered the lock, water is evacuated out of the lock. As a result, the pressure difference between the fore and aft part of the ship decreases, reducing the oscillations. The hydrodynamic force Y and the moment N also shows the same tendency. Bank effect develops in case of an eccentric approach until the ship has entered the lock. The asymmetric flow around the ship induced by the vicinity of banks causes pressure differences between port and starboard sides. The velocity will increase alongside the nearest bank, causing a pressure decrease. As a result, a lateral force will act on the ship, directed towards the closest bank, as well as a yawing moment pushing the ship bow toward the center of the waterway. Once the ship has entered the lock, the asymmetric flow disappears and the lateral force, as well as the yawing moment falls to zero. This is confirmed by the results shown in Figs. 8(b) and 8(c).

Int. J. Comput. Methods 2016.13. Downloaded from www.worldscientific.com
by SHANGHAI JIAOTONG UNIVERSITY on 07/27/16. For personal use only.

4.2. *Vertical displacements*

Piston effect, which provokes an accumulation of water during entry into a lock, causes the increase of the return flow velocity and a sinkage of the water level in the vicinity of the ship, which induces a general sinkage of the ship. The return flow of the ship causes a pressure drop around the ship, according to the Bernoulli principle. As a result, the ship also moves vertically downward. Generally, the pressure drop will not be distributed equally over the ship, causing a trim.

The mean sinkage σ and trim τ were determined from the calculated sinkage force Z and trim moment M using the formulae (positive sinkage upwards and positive trim bow-up):

$$\sigma = Z/\rho g A_w, \tag{15}$$

$$\tau = M/\rho g I_w, \tag{16}$$

where A_w denotes the water plane area and I_w represents the longitudinal moment of inertia of the water plane area about the center of floatation. The vertical displacement of the fore and aft perpendiculars zFP and zAP can be computed by:

$$zFP + zAP = 2\sigma, \tag{17}$$

$$zFP - zAP = L_{PP}\tau. \tag{18}$$

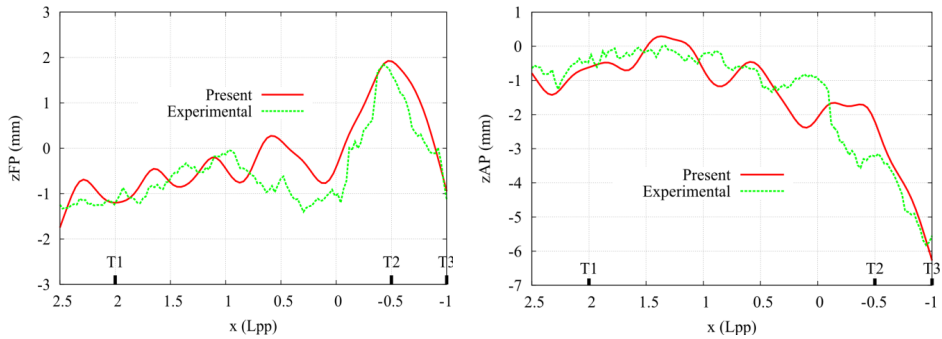

(a) Time history of *zFP*

(b) Time history of *zAP*

Fig. 9. Time history of *zFP* and *zAP*.

Int. J. Comput. Methods 2016.13. Downloaded from www.worldscientific.com
by SHANGHAI JIAOTONG UNIVERSITY on 07/27/16. For personal use only.

Figure 9 reports the vertical displacement of the fore and aft perpendiculars. Reasonable correspondence between the computational and experimental data can be noted.

Three stages in the development of *zFP* are shown in Fig. 9(a). First, negatively *zFP*, which is caused by the shallow water effect, with insignificant oscillation is noticed when the ship maneuvers in the approach channel. This is caused by the low speed. Then, an initial rising of the bow, which might be caused by the accumulation of water in front of the ship, can be noticed when the ship entering the lock. Third, once more than half of the vessel is inside of the lock, the sinkage oscillation of *zFP* decreased. This is induced by the evacuation of the water in the lock. When the ship has entered the lock, the sinkage of the bow disappears. Figure 9(b) manifests that the vertical displacement of the aft perpendiculars *zAP* is increasing as the ship entering the lock. This might be caused by the continuous declination of the surface pressure of the aft-body of the ship. The increasing of the relative speed between ship and return flow, as well as the sinkage of water level around the stern induce the decrease of the surface pressure of the aft-body of the ship, so that the aft perpendiculars moves vertically downward.

The results of hydrodynamic forces and moments, as well as the vertical displacements show good agreement with the experimental data, which demonstrates that FDM method can accurately simulate the viscous flow around the ship with relatively small amounts grids. The results also indicate that the currently used numerical methods are suitable for studying the viscous flow around the ship during the entering maneuver into a lock with different eccentricity, which is presented in the next section.

4.3. *Water level elevation and wave profile*

For a better understanding of the physical mechanisms, which cause the interesting phenomenon when a ship maneuvers into a lock, a sketch of the water level elevation,

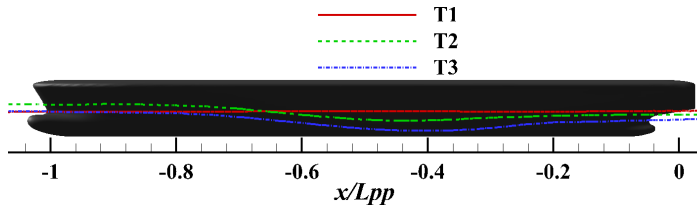

Fig. 10. Water level elevation around the ship at different time for benchmark case.

Int. J. Comput. Methods 2016.13. Downloaded from www.worldscientific.com
by SHANGHAI JIAOTONG UNIVERSITY on 07/27/16. For personal use only.

plotted at the plane $y/Lpp = -0.078$, and the wave profile along port side of the hull at three different instants T1, T2, T3 is shown in Figs. 10 and 11, respectively. The water level elevation in Fig. 10 is multiplied by 10 for clarity. In Fig. 11, the $x/L_{pp} = -1$ phase is defined at the fore perpendicular of the ship. Due to the low ship speed, at time T1 the free surface around the hull is nearly flat, so that the hydrodynamic force X, as shown and discussed in Fig. 8(a), is very small with insignificant oscillation when the ship maneuvers in the approach channel. At time T2, higher water level elevation around the fore-body and lower water level around the aft-body are noticed, which might be caused by the accumulation of water in front of the bow. This causes the increase of the surface pressure on the fore-body and the decrease of the surface pressure of the aft-body, which induces an initial rising of zFP and further decrease of zAP. This is also confirmed by the results shown in Fig. 9. Decrease of the water level elevation in the vicinity of the ship is noticed at time T3, which indicates that the water in front of the ship is being evacuated out of the lock. This causes a decrease of the hydrodynamic force in x-direction X as well as a pressure drop around the ship. This further induces the

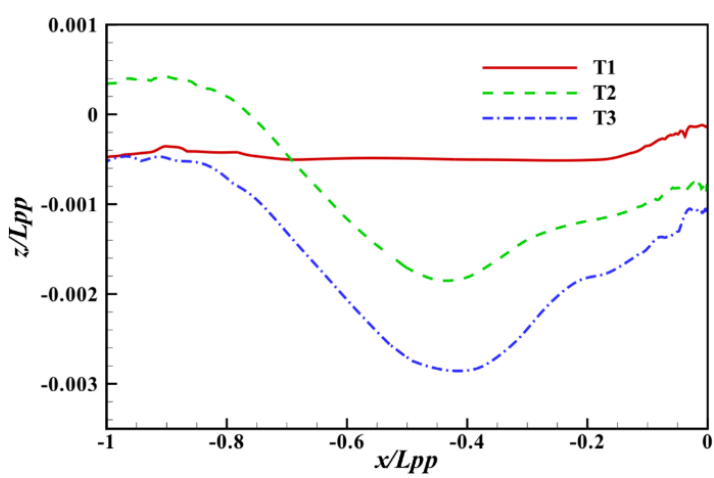

Fig. 11. Wave profile along port side of the hull at three different time.

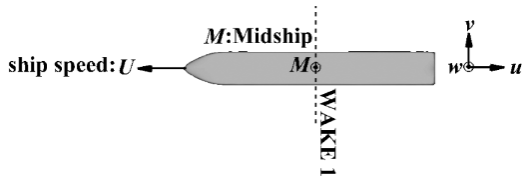

Fig. 12. Coordinate systems for velocity fields.

vertical displacement of the fore and aft perpendiculars zFP and zAP, which also supports the results and discussion of Figs. 8 and 9.

Int. J. Comput. Methods 2016.13. Downloaded from www.worldscientific.com
by SHANGHAI JIAOTONG UNIVERSITY on 07/27/16. For personal use only.

4.4. *Wake*

Figure 12 presents the coordinate systems for velocity fields and the measurement plane — WAKE 1 plane, which cuts through $x/L_{pp} = 0.5$ at the centerline of the hull. The axial velocity, u, plotted at WAKE 1 plane ($x/L_{pp} = 0.5$) at instants T1, T2 and T3 is shown in Fig. 13. The effect of high blockage on the velocity of the return flow is revealed. Due to the shallow water effect, a minor increase of the axial velocity of the return flow is noticed at instant T1. At instant T2, the wake field is much different with the wake field at instant T1. First, as a result of the high blockage, a significantly increased axial velocity of the return flow is noted. Second, due to the eccentric approach, the velocity of the return flow at port and starboard

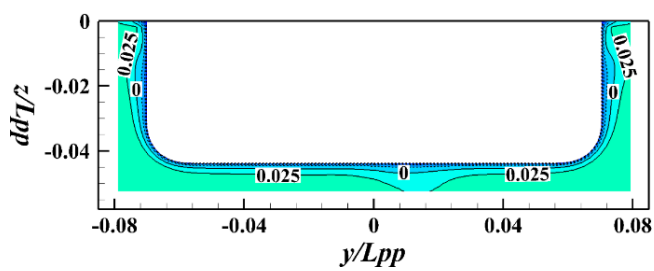

(a) instant T1

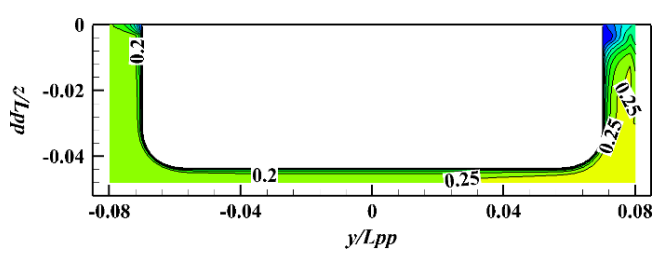

(b) instant T2

Fig. 13. Velocity field contours in WAKE 1 plane for benchmark case.

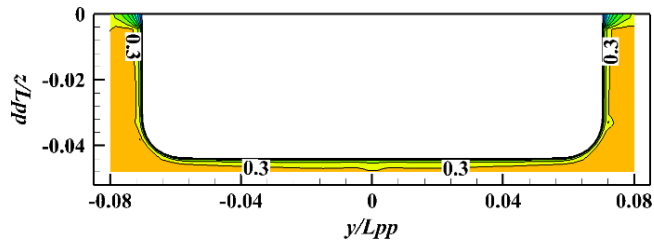

(c) instant T3

Fig. 13. (*Continued*)

Int. J. Comput. Methods 2016.13. Downloaded from www.worldscientific.com
by SHANGHAI JIAOTONG UNIVERSITY on 07/27/16. For personal use only.

sides is different, which might causes the different surface pressure of the ship sides and a lateral force is produced accordingly. Due to the symmetric flow field around the ship at instant T3, the velocity shows symmetrical character, which means that the wake field around the ship becomes neat. A significant increase of the amplitude of velocity at instant T3 is also noticed in Fig. 13(c).

4.5. *Surface pressure distribution*

The computational results showing the pressure distributions on the hull surface at instants T1, T2 and T3 for the benchmark case are presented in Figs. 14–16.

The increasing blockage coefficient during the entering maneuver of a ship into a lock, induces an increase of relative speed between the ship and return flow, which causes a general reduce of the surface pressure. However, Fig. 15 reveals a significant increase of the pressure of the fore part of the hull at instant T2, which causes the increase of the longitudinal force as well as the rising of the bow, as shown in Figs 8(a) and 9(a). This is caused by the accumulation of water in front of the ship. Furthermore, the accumulation of water in front of the ship is evacuated out of lock at instant T3. This leads to a decrease of the surface pressure, which is confirmed by Fig. 16. Besides, the decrease of the surface pressure of the fore part causes the sinkage of the bow, which is shown in Fig. 9(a). Moreover, negative pressure is

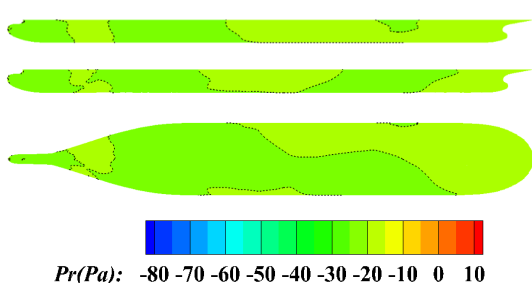

Fig. 14. Surface pressure (port side view, starboard side view and top view) for benchmark case at instant T1.

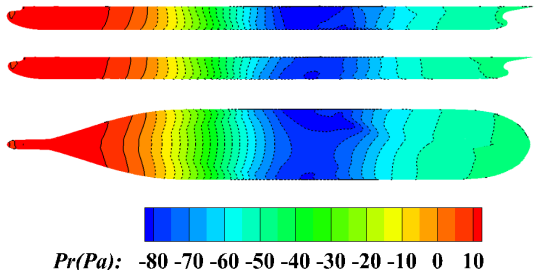

Fig. 15. Surface pressure (port side view, starboard side view and top view) for benchmark case at instant T2.

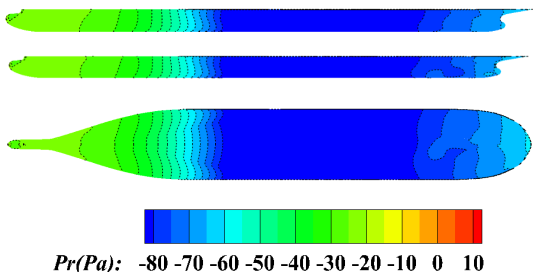

Fig. 16. Surface pressure (port side view, starboard side view and top view) for benchmark case at instant T3.

always noticed on the aft part of the hull surface during the whole process. This explains the increasing oscillation of the sinkage of the aft perpendiculars zAP, which is presented in Fig. 9(b). On the other hand, due to the eccentric approach the pressure distribution on the two sides of the ship become asymmetric. At instant T2, the starboard-side pressure is lower than that on the port-side after the parallel middle body, which produces a lateral force towards the starboard and a positive yaw moment will turn the hull toward the starboard-side.

5. Results of Systematic Computations

The effect of eccentricity on the characteristic of the viscous flow around the ship, during the entering maneuver of a ship into a lock is significant. In order to give a clear insight into the ship behavior when the ship moves into the lock with different eccentricity, case A1 and case A2 were carried out. The details of the test conditions for the systematic study are given in Table 2.

5.1. *Hydrodynamic forces*

Figure 17 presents the hydrodynamic forces and moment of the 12000TEU ship model when entry into the lock with different lateral position. All the results show that the eccentricity increases do not alter the general pattern of the forces and

Int. J. Comput. Methods 2016.13. Downloaded from www.worldscientific.com
by SHANGHAI JIAOTONG UNIVERSITY on 07/27/16. For personal use only.

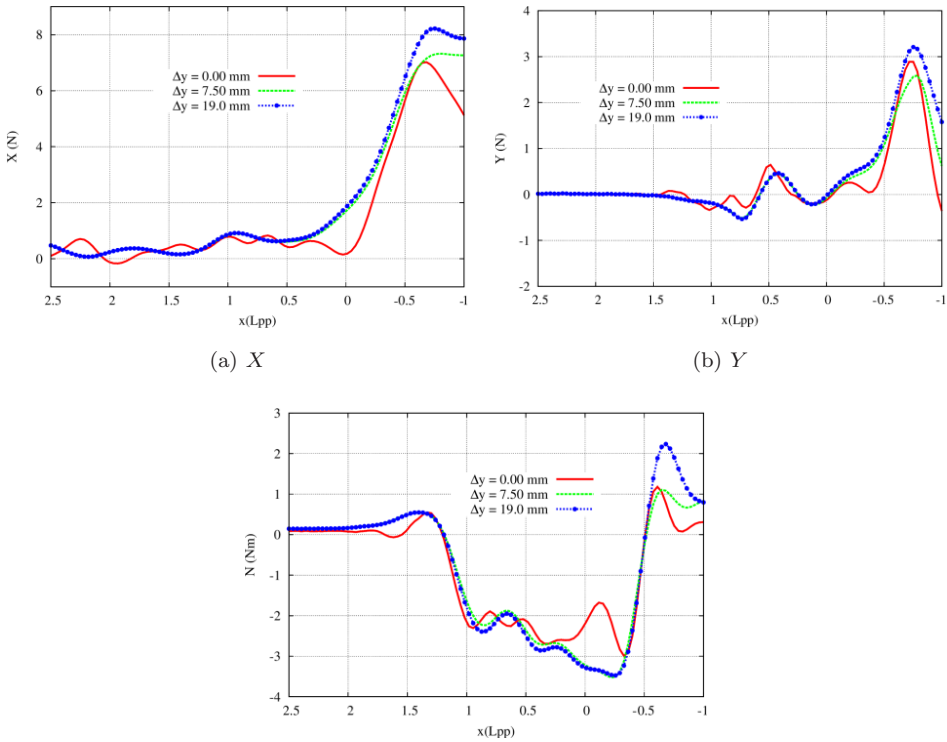

(a) X (b) Y

(c) N

Fig. 17. Time history of the hydrodynamic forces and moment for different eccentricity cases.

Int. J. Comput. Methods 2016.13. Downloaded from www.worldscientific.com
by SHANGHAI JIAOTONG UNIVERSITY on 07/27/16. For personal use only.

moment, but just cause higher extreme values. The results declare that more pronounced prevention of water in the lock from evacuate out can be noticed with increasing eccentricity. So, more water in the lock might be accumulated in the lock, which causes higher velocities of the return flow. Accordingly, the longitudinal force X increases. Furthermore, the flow around the ship will be more asymmetric with higher eccentricity. As the ships are allowed with very small side margins in the lock, higher eccentricity represents higher risk of collision of ship and side walls. So, protection measures, such as fenders, are suggested.

5.2. *Vertical displacements*

The vertical displacement of the fore and aft perpendiculars zFP and zAP for different lateral position are computed and presented in Fig. 18. Both of zFP and zAP increase with increasing eccentricity. This causes higher risk of bottom touch. Due to the high blockage of the lock, especially the shallow water effect, the increase of the risk of bottom touch is noteworthy. According to the results, moving along the lock's centerline is the safest way when maneuvering into a lock.

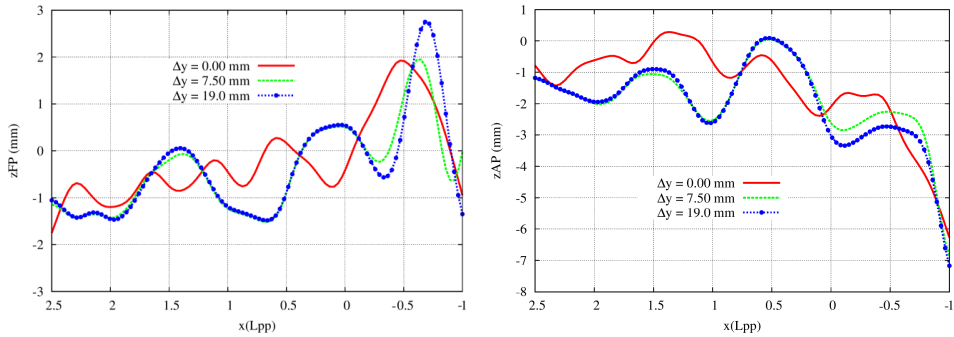

(a) Time history of zFP (b) Time history of zAP

Fig. 18. Time history of zFP and zAP for different eccentricity cases.

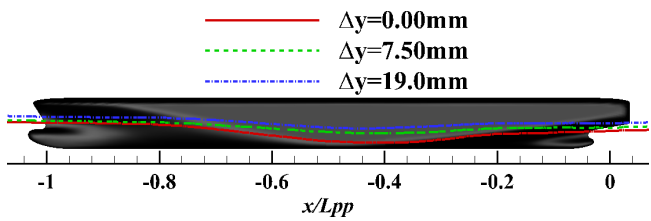

Fig. 19. Water level elevation around the ship for different ship speed cases.

5.3. *Water level elevation and wave profile*

A depiction of the water level elevation around the ship, plotted at plan $y/Lpp = -0.078$, at time T3 for different eccentricity cases is give in Fig. 19, where the water level elevation is multiplied by three for clarity. Figure 20 presents the wave profile of the port side of the ship at time T3 for different eccentricity cases. The general pattern of the wave profile does not change. However, higher water elevation around the ship with increasing eccentricity is noticed. The results shown in Figs. 17 and 18 prove that it is more difficult for water to be evacuated out with higher eccentricity. First, this leads to higher water level elevation in the lock, which induces higher relative speed between the ship and return flow. The higher velocity of the return flow causes an increased frictional resistance. Moreover, the higher velocity of the return flow results in a pressure drop, which induces a general sinkage.

5.4. *Wake*

The computed results of the wake at WAKE 1 plane at instant T3 for different eccentricity cases are shown in Fig. 21. Both Figs. 21(b) and 21(c) reveal an asymmetric flow, while Fig. 21(a) shows a symmetric flow around the ship. As a result, the lateral force as well as the yawing moment was supposed to be

Int. J. Comput. Methods 2016.13. Downloaded from www.worldscientific.com
by SHANGHAI JIAOTONG UNIVERSITY on 07/27/16. For personal use only.

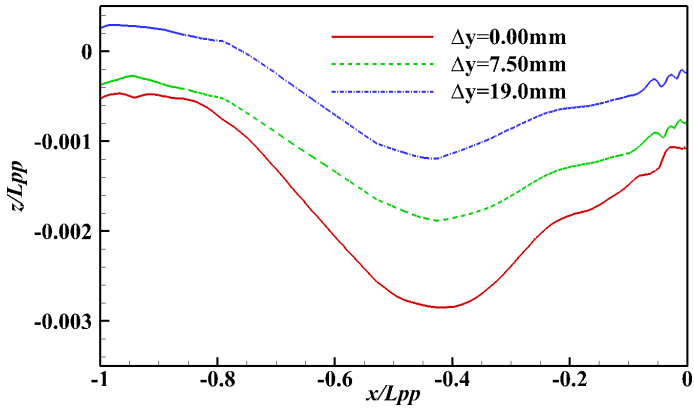

Fig. 20. Wave profile along port side of the hull at time T3 for different ship speed.

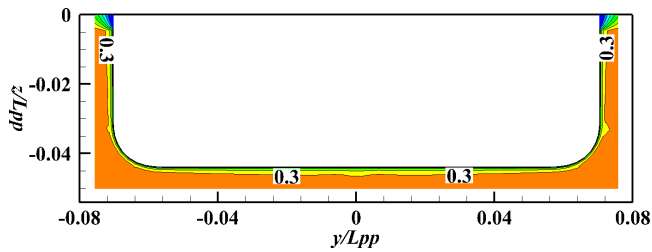

(a) $\Delta y = 0.0\,\mathrm{mm}$

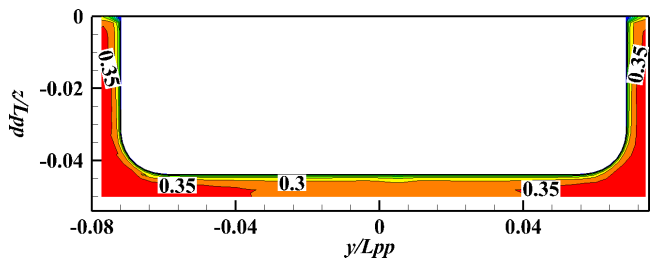

(b) $\Delta y = 7.5\,\mathrm{mm}$

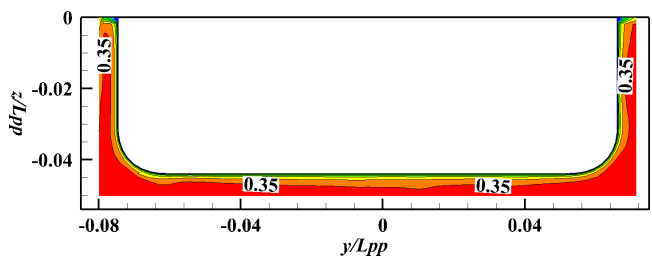

(c) $\Delta y = 19\,\mathrm{mm}$

Fig. 21. Velocity field contours in WAKE 1 plane at time T3 for different eccentricity cases.

Int. J. Comput. Methods 2016.13. Downloaded from www.worldscientific.com
by SHANGHAI JIAOTONG UNIVERSITY on 07/27/16. For personal use only.

nonzero for cases A1 and A2. On the other hand, due to the high blockage, higher velocity of the return flow is observed with higher eccentricity. With smaller side margin, it is much more difficult to evacuate the accumulated water in front of the ship.

5.5. *Surface pressure distribution*

Figure 22 presents the computed results of the surface pressure at time T3 for different eccentricity cases. First, higher surface pressure around fore-body than that around aft-body is shown in all cases. This is causes by the higher water level elevation in the vicinity of the fore-body. Second, the results also manifest that the surface pressure, as well as the asymmetry of the surface pressure increases with increasing eccentricity. The difference of surface pressure between port and starboard sides is mainly concentrated in the aft-body of the hull and the surface pressure on the starboard side is larger than that on the port side. As a result, a negative yaw moment will turn the hull toward the starboard-side.

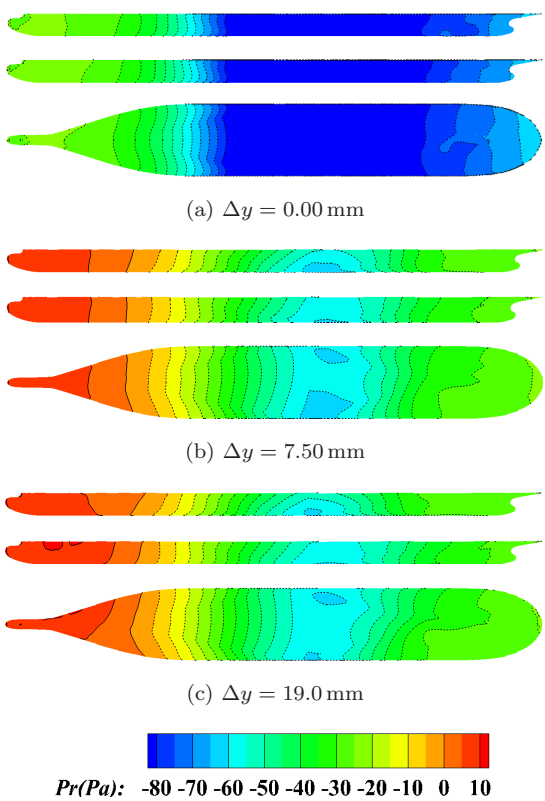

Fig. 22. Pressure (port side view, starboard side view and top view) against different ship speed at instant T3.

Int. J. Comput. Methods 2016.13. Downloaded from www.worldscientific.com
by SHANGHAI JIAOTONG UNIVERSITY on 07/27/16. For personal use only.

Int. J. Comput. Methods 2016.13. Downloaded from www.worldscientific.com
by SHANGHAI JIAOTONG UNIVERSITY on 07/27/16. For personal use only.

6. Conclusion

Effects of eccentricity on the hydrodynamics of a ship entering a lock were investigated and reported in this paper. The capability of the present method for the prediction of the viscous flow around the ship model entering the lock is confirmed by the good agreement of the predicted results with the corresponding experimental data. The hydrodynamic forces, vertical displacements as well as surface pressure distribution were presented and discussed. A significant effect of eccentricity on the hydrodynamic forces and moment, as well as ship sinkage was noticed. Furthermore, FDM method is especially suitable for solving low speed headache with remarkable free surface effects. The results also show the unparalleled advantages of CFD, such as physical insight, in investigating ship behavior in locks. CFD can be a useful tool to investigate ship–lock interactions.

The systematic investigations were then made to examine the effects of the eccentricity on the hydrodynamics on the ship when it enters a lock. According to the results, several interesting observations can be made:

1. Hydrodynamic forces and moment, as well as the sinkage of the ship are sensitive to the eccentricity.
2. Hydrodynamic forces and moment, as well as the sinkage of the ship, increase with increasing eccentricity. This causes the increases of the difficulty to maneuver a ship into a lock, safely.
3. When the eccentricity increases, an increase of the risk of side collision is observed.
4. When entering a lock, moving along the lock's centerline and protection measures is suggested.

Acknowledgments

This work is supported by National Natural Science Foundation of China (Grant Nos. 51379125, 51490675, 11432009, 51411130131 and 11272120), The National Key Basic Research Development Plan (973 Plan) Project of China (Grant No. 2013CB036103), High Technology of Marine Research Project of The Ministry of Industry and Information Technology of China, Chang Jiang Scholars Program (Grant No. T2014099) and the Program for Professor of Special Appointment (Eastern Scholar) at Shanghai Institutions of Higher Learning (Grant No. 2013022), to which the authors are most grateful.

References

Chen, X. N. [2010] "From water entry to lock entry," *J. Hydrodyn. Ser. B* **22**(5), 885–892.

Delefortrie, G., Willems, M. *et al.* [2008] "Tank test of vessel entry and exit for third set of Panama locks," In *Proc. Int. Navigation Seminar following PIANC AGA*, Beijing, China, pp. 517–523.

Delefortrie, G., Willems, M. *et al.* [2009] "Behavior of post panamax vessels in the third set of panama locks," In *Int. Conf. Marine Simulation and Ship Maneuverability (MARSIM'09, Panama City, Panama).*

Meng, Q. J. and Wan, D. C. [2014] "Numerical simulations of ship motions in confined water by overset grids method," In *The 24th Int. Ocean and Polar Engineering Conf.,* Busan, Korea, Vol. 3, pp. 463–469.

Meng, Q. J. and Wan, D. C. [2015] "Numerical simulations of viscous flows around a ship while entering a lock with overset grid technique," In *The 25th Int. Ocean and Polar Engineering Conf.*, Hawaii, USA, Vol. 4, pp. 989–996.

Menter, F. R. [1994] "Two-equation eddy-viscosity turbulence models for engineering applications," *AIAA J.* **32**(8), 1598–1605.

Osher, S. and Sethian, J. A. [1988] "Fronts propagating with curvature-dependent speed: Algorithms based on Hamilton–Jacobi formulations," *J. Comput. Phys.* **79**(1), 12–49.

Richter, J., Verwilligen, J. *et al.* [2012] "Analysis of full ship types in high-blockage lock configurations," In MARSIM 2012, Singapore, pp. 1–9.

Sethian, J. A. and Smereka, P. [2003] "Level set methods for fluid interfaces," *Annu. Rev. Fluid Mech.* **35**(1), 341–372.

Sussman, M., Smereka, P. and Osher, S. J. [1994] "A level set approach to computing solutions to incompressible two-phase flow," *J. Comput. Phys.* **114**(1), 146–159.

Vantorre, M., Delefortrie, G. and Mostaert, F. [2012] "Behavior of ships approaching and leaving locks: Open model test data for validation purposes," Version 2.1, WL Rapporten, WL2012R815_08e, Flanders Hydraulics Research and Ghent University, Division of Maritime Technology, Antwerp, Belgium.

Vergote, T. [2012] "Hydrodynamics of a ship while entering a lock," Eng. thesis, Ghent University, Ghent, Belgium.

Vrijburcht, A. [1988] "Calculations of wave height and ship speed when entering a lock," *Delft Hydraul. Publ.* **391**, 1–17.

Wang, H. Z. and Zou, Z. J. [2014] "Numerical study on hydrodynamic interaction between a berthed ship and a ship passing through a lock," *Ocean Eng.* **88**, 409–425.

Int. J. Comput. Methods 2016.13. Downloaded from www.worldscientific.com
by SHANGHAI JIAOTONG UNIVERSITY on 07/27/16. For personal use only.